*J. Fluid Mech.* (1993), *vol.* 246, *pp.* 419–442



# The effect of a circular cylinder on the diffusion of matter by a plume

By H. TSUNODA, Y. SAKAI, I. NAKAMURA AND S. LIU†
Department of Mechanical Engineering, Nagoya University, Nagoya 464-01, Japan

(Received 2 January 1990 and in revised form 15 July 1992)

Experimental results are given for the mean and fluctuation concentration in a plume from a point source in grid-generated turbulence, which has developed so as to have a width comparable to the cylinder diameter, is disturbed by a cylinder with its axis intersecting the plume axis perpendicularly. It is shown that the disturbance effect of the cylinder appears in the upstream region of about 1.5 diameter from the stagnation point. As the stagnation point is approached, the increased travel time and the enhanced molecular diffusion cause a noticeable amplification of the dissipation of concentration variance. Also, the characteristics of some conditional statistics of the plume entrained in the wake are examined in order to investigate the intermittent structure of the plume meandering produced by the Kármán vortex street.

## 1. Introduction

The diffusion of matter in turbulent flow is one of the most important problems in engineering and meteorology, and many practical diffusion problems occur in complex turbulent shear flows disturbed by obstacles such as mechanical elements or buildings and hills. It is well known that various fluid dynamical characteristics of such complex flows, for example convergence and divergence of mean streamlines and the inhomogeneity of turbulence, affect in a complicated way the diffusion field developed inside them (Hunt, Britter & Puttock 1979).

There have been extensive experiments to measure the mean concentration of air pollution around or behind a simply shaped obstacle in turbulent flow, when the source of pollution is placed near the obstacle. Puttock (1979) measured the concentration of gas released from a line source which is placed inside or outside the separated recirculating region behind a circular cylinder in grid-generated turbulence and compared his results with the theoretical prediction based on the diffusion equation by Puttock & Hunt (1979). Robins & Castro (1977), Ogawa & Oikawa (1982) and Ogawa, Oikawa & Uehara (1983) measured the mean concentration of a plume from a point source near a cube placed in a turbulent boundary layer. They showed the effects of mean flow direction and upwind turbulence level.

While the above studies mainly focus on the diffusion field downstream of the body, there has been little research on the upstream region where the turbulence distortion by the body is considered to be crucial for the development of the plume. In 1973, Hunt & Mulhearn developed a Lagrangian statistical theory for the problem of turbulent diffusion in straining flow around a two-dimensional body, when the

† Present address: Research and Development Division, ULVAC Japan Co. Ltd., Chigasaki, Kanagawa 253, Japan.

FIGURE 1. A photograph showing plume distortion upstream of the cylinder.

source of the scalar is placed near and upstream of the body. They provided the mean-square dispersion of the plume relative to the mean streamline which passes the source. Hunt *et al.* (1979) extended this theory to the diffusion problem in a three-dimensional straining flow. Keffer *et al.* (1978) examined experimentally how the thickness of a two-dimensional thermal mixing layer changes in a region of converging streamlines, although they did not use an obstacle to generate the straining flow.

The purpose of this study is to examine experimentally the disturbance effect of a circular cylinder on the diffusion process of a plume from a point source in grid-generated water turbulence. The source of matter is located far upstream of the cylinder so that the width of the impinging plume is comparable to the cylinder diameter. Similar experiments have been conducted by LaRue & Libby (1974) and Fabris (1979), who investigated the temperature field in the wake of a heated cylinder. But it must be noted that their experiments differ somewhat from the present one, because the developing region of the scalar from the heated cylinder is the same as that of the turbulent wake (if the molecular diffusion can be neglected).

In the present study, experimental results have been obtained for the mean and fluctuation concentration as well as the velocity field upstream of, around and behind

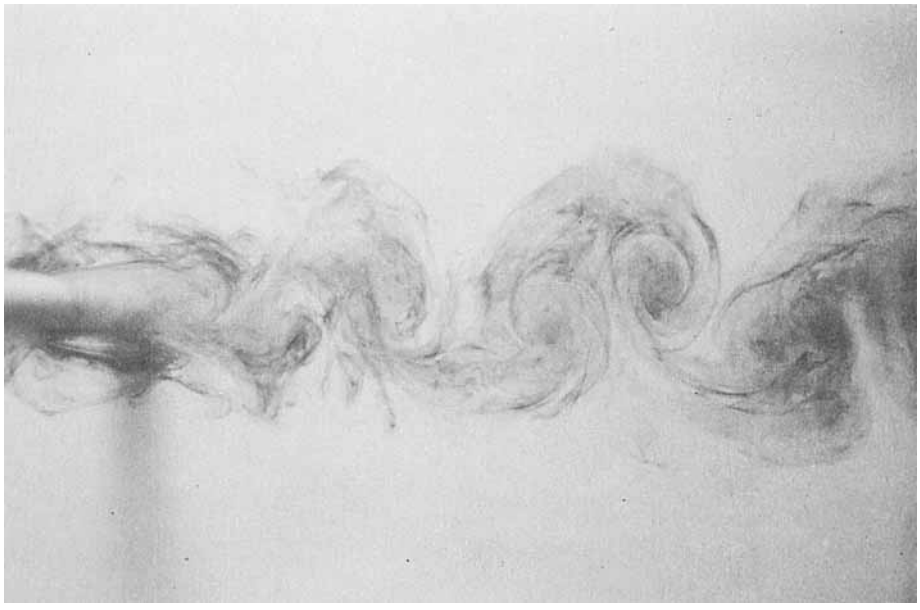

FIGURE 2. A photograph showing a vortex entrained plume downstream of the cylinder.

the cylinder. In particular, we have given much attention to two significant effects of the obstacle on the diffusing plume; that is, the effect of the flow distortion around the cylinder, and the effect of the inhomogeneous and large-eddy turbulence downstream of the cylinder. The above two effects seem to be crucial in the disturbance effect of the cylinder on the plume. Figure 1 shows an example of a distorted plume just upstream of the cylinder, indicating how the plume, which has developed in grid-turbulence, is rapidly distorted close to the cylinder surface. On the other hand, figure 2 demonstrates a typical pattern of the plume downstream of the cylinder. The diffusing matter which is entrained into the vortex shedding wake evolves as a kind of meandering plume with an instantaneous centre of mass varying periodically (see, for example, Hanna 1984). In this paper, some detailed experimental data specially concerned with the above two effects on the mean and fluctuating concentration field will be given separately in §4.2.1 and §§4.2.2 and 4.2.3. The characteristics of some conditional statistics of the plume entrained in the wake will be also examined in order to show the intermittent structure of the plume meandering as shown in figure 2.

## 2. Experimental apparatus and conditions

Figure 3 shows a schematic of the working section and coordinate systems. The test section was an open channel 250 mm high, 250 mm wide and 1960 mm long. The water depth $h_w$ in the working section was adjusted to $170 \pm 0.2$ mm from the bottom. At the entrance to the working section a biplanar square grid was placed with mesh length $M = 10$ mm and bar-to-mesh ratio 1:5. The diffusing matter (an aqueous solution of D.F. orange (direct dye)) was injected from a nozzle with exit diameter 2 mm. The exact value of the molecular diffusivity for this dye solution is unknown, but it is expected to be of order $10^{-10}$ m$^2$/s. The nozzle was soldered to a pipe which replaced one of the vertical rods of the grid, and its exit was located

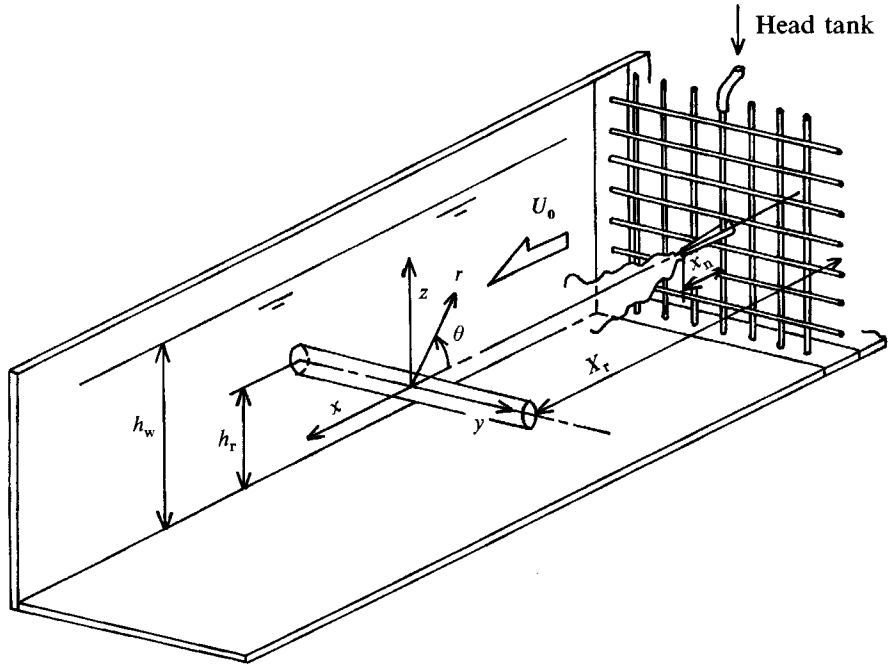


FIGURE 3. Schematic of the working section and coordinate systems.

$x_n = 20$ mm downstream of the grid. The injection velocity of the dye solution was about 1.7 times that of the main flow. This velocity was selected so as to cancel the momentum defect due to the wake of the nozzle (see Nakamura, Sakai & Miyata 1987 hereafter referred to as NSM). The decay of turbulence fluctuations in the grid turbulence and the characteristics of the mean and fluctuating concentration fields from a point source have been already reported by NSM.

The diameter $d$ of the circular cylinder used as an obstacle is 10 mm. The cylinder was fixed horizontally to the channel wall at $x_r = 350$ mm downstream of the grid as shown in figure 3. The half-width of the plume in the absence of the cylinder was about $0.75\,d$ at the cylinder location. The mean velocity of the main flow $U_0$ is about 13.9 cm/s, so that Reynolds number $Re_M = U_0 M/\nu$ and $Re_d = U_0 d/\nu$ are both about 1064, where $\nu$ is the kinematic viscosity and we adopted $\nu = 1.307$ mm$^2$/s at 10 °C. As shown in figure 3, the coordinate systems $x$, $y$, $z$ and $r$, $\theta$ are used, where $\theta$ is measured from the plume axis.

The mean velocity field was measured by a laser-Doppler velocimeter (KANOMAX, Model 27-0900 series) and the output signals were processed by a tracker-type signal processor (KANOMAX, Model 27-1090A). The streamwise velocity fluctuations were measured by a cylindrical hot-film probe (TSI, Model 1212-20W; the diameter and length of the sensing part are 52 μm and 1 mm, respectively) in conjunction with a constant-temperature velocity anemometer (HAYAKAWA, Model HC-30).

The concentration fields were measured by our own concentration fluctuation measuring system (see Nakamura, Miyata & Sakai 1983) incorporating a light absorption method. Light from a tungsten lamp is introduced into a sampling volume where the light intensity is reduced according to the instantaneous concentration of the diffusing matter existing in the volume. A photomultiplier is used to convert the intensity of the modified light to the voltage output. A typical

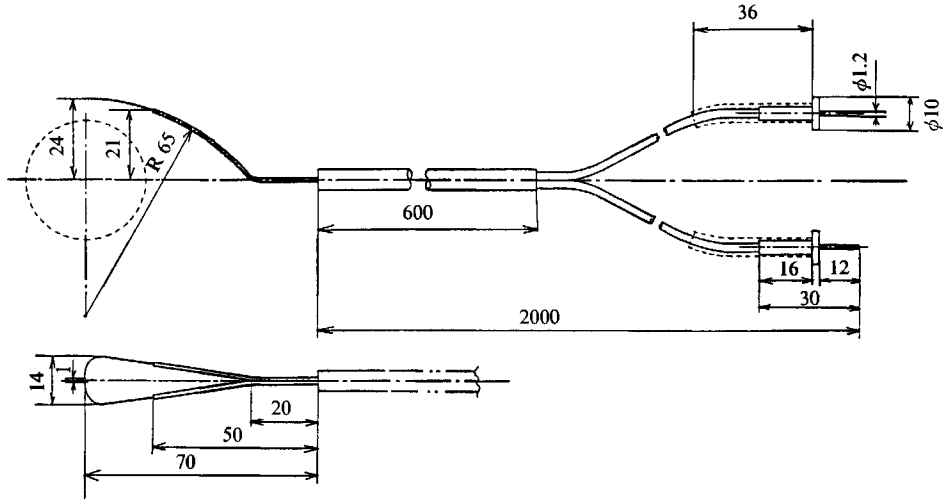


FIGURE 4. Schematic sketch of the light probe; dimensions in mm.

signal–noise ratio is about 40 dB for the concentration signal measured at a point on the plume axis. Prior to the experiment, the existence of an approximate linear relation between the concentration value and the corresponding voltage output was confirmed, when the concentration is less than a limiting value. The experiment is conducted under the condition that the instantaneous concentration does not exceed this limiting value. Figure 4 is a sketch of the light probe for measurement of the concentration around the cylinder. The stainless-steel tube, through which the bundle of glass fibres passes, has a curvature in order to make it possible to perform the measurements close to the stagnation point of the cylinder. The diameter of the bundle is 0.5 mm and the sampling length was adjusted to about 1.0 mm. Therefore, the sampling volume of the light probe was about 0.2 mm$^3$. The output signals of the concentration measuring circuit were sampled by an AD-converter (sampling frequency 5 kHz) and then processed by a computer. Although the frequency response of the measuring circuit may possibly be over 10 kHz, the most important factor in estimating the time response is considered to be the sampling volume of the probe (Chatwin & Sullivan 1987). The Kolmogorov scale $\eta$ in our grid turbulence is estimated to be about 0.6 mm (NSM) and thus the Batchelor scale $\eta_\gamma \equiv \eta/Sc^{\frac{1}{2}}$ of our scalar field is expected to be of order $10^{-2}$ mm ($Sc$ is the Schmidt number and we used $Sc \sim 10^3$). Therefore, our light probe could resolve the spatial concentration fluctuation down to the Kolmogorov scale.

The factors that determine the characteristics of the velocity and concentration fields in this experiment are considered to be the following four non-dimensionalized parameters (Hunt & Mulhearn 1973; Kiya *et al.* 1982): $Re_d$, $u_0'/U_0$, $L/d$ and $b_T/d$, where $u_0'$ and $L$ are the r.m.s. value of the longitudinal velocity fluctuation and the longitudinal integral scale of the mainstream turbulence, respectively, and $b_T$ is the half-width of the plume without the cylinder. As mentioned above, the Reynolds number was $Re_d = 1064$ and the ratio of the plume half-width to the diameter was about $b_T/d = 0.75$ at a downstream distance $x_r/M = 35$ from the grid, which corresponds to the cylinder location. At the same location, $u_0'/U_0$ and $L/d$ without the cylinder were about 0.019 and 0.8, respectively. Although it is well known that the structure of the flow and turbulence field around the cylinder is significantly

affected by these parameters, results for only one combination of parameters are presented here. In addition, it should be noted that the Reynolds number in this experiment is rather small in comparison with full-scale phenomena such as diffusion around hills and buildings.

## 3. The method of conditional sampling

A statistic that characterizes the intermittent plume observed in this experiment is the intermittency function $\tilde{I}(t)$ with respect to the instantaneous concentration of scalar $\tilde{\Gamma}(t)$, defined by the following relation (O'Brien 1978):

$$\tilde{I}(t) = \begin{cases} 1 & \text{if} \quad \tilde{\Gamma}(t) > 0 \\ 0 & \text{if} \quad \tilde{\Gamma}(t) = 0. \end{cases} \tag{1}$$

In this section, the method of conditional sampling adopted will be briefly summarized (for details, see Nakamura, Sakai & Tsunoda 1989). This method is broadly composed of two steps, A and B. In step A, the intermittency factor $I_\Gamma$, defined as the time average of $\tilde{I}(t)$, is directly estimated from the probability density function of $\tilde{\Gamma}(t)$ (Bilger, Antonia & Sreenivasan 1976). Because the concentration signal from the measuring system has an inevitable electronic noise, the p.d.f. of the noise-contaminated concentration signal includes a contribution from the noise. Now, assuming the noise to be Gaussian, the contaminated concentration signal $\tilde{E}$ can be expressed by $\tilde{E} = E_0 + \alpha\tilde{\Gamma} + e'_n\xi$. $E_0$ is a signal level corresponding to $\tilde{\Gamma} = 0$, $e'_n$ is an r.m.s. value of noise, $\alpha$ is a proportionality constant (which is determined from the calibration) and $\xi$ is a standardized Gaussian random variable which is independent of $\tilde{\Gamma}$. After decomposing the p.d.f. of $\tilde{\Gamma}$ into two conditional p.d.f.s based on the intermittency factor, the p.d.f. of the noise-contaminated concentration signal is given by

$$P(\tilde{E}) = \frac{1-I_\Gamma}{e'_n(2\pi)^{\frac{1}{2}}} \exp\left\{-\frac{(\tilde{E}-E_0)^2}{2e'^2_n}\right\} + I_\Gamma \int_{-\infty}^{\infty} \frac{1}{e'_n(2\pi)^{\frac{1}{2}}} \exp\left\{-\frac{(\tilde{E}-\tilde{E}')^2}{2e'^2_n}\right\} P_t(\tilde{E}')\,\mathrm{d}\tilde{E}', \tag{2}$$

where $P_t$ is a true conditional p.d.f. of the concentration signal without the noise (the p.d.f. of $\tilde{\Gamma}$ conditioned on $\tilde{I} = 1$). If $e'_n$ is far less than the r.m.s. value of $P_t$ (this means a high signal-to-noise ratio), the second term in (2) may be simply approximated by $I_\Gamma P_t(\tilde{E})$. Then the contribution of the noise is expressed by the Gaussian shown by the first term and the area under this Gaussian is equal to $1-I_\Gamma$. Accordingly, the intermittency factor can be estimated by finding a best-fitted Gaussian curve to the noise part of the measured p.d.f. Since the signal-to-noise ratio in the present concentration signal was not enough large to satisfy the above condition, we used the next step, B, together with this step A in order to make the conditional processing more accurate.

In the step B, the intermittency function $\tilde{I}(t)$ is determined by using a threshold level and a hold time (LaRue 1974). Here, the threshold level $S$ is given by

$$S = E_0 + ke'_n, \tag{3}$$

where $k$ is a threshold parameter. We determined the value of $k$ by comparing the intermittency factor obtained from step A with that obtained from this step B as the time average of the intermittency function. It was found that when $k$ equals 1.7, both intermittency factors from the two steps coincide well.

The intermittency function obtained from (3) is still rather spiky owing to the electronic noise. Therefore, this spiky intermittency function was corrected by using a hold time $\tau_h$ so that the corrected intermittency function does not have a time fluctuation higher than the cutoff frequency $\tau_h^{-1}$. Because we need only the time average of the intermittency function, the relatively large value $\tau_h = 2$ ms was used.

Verification of the conditional sampling adopted in this study was made by visual comparison between the intermittency function $\tilde{I}(t)$ from step B and the concentration signal $\tilde{\Gamma}(t)$.

## 4. Experimental results and discussion

### 4.1. *Velocity fields*

Figure 5 shows the $z$-direction distributions of the r.m.s. longitudinal velocity fluctuation values $u'$ at $x/d = -1.6$, $-3.0$, $-5.0$ upstream of the cylinder. The homogeneity of the upstream turbulence is seen to be moderately good in the core region $-2 < z/d < 2$ except for the top and bottom regions of the channel where the turbulence is inhomogeneous, probably due to the developing turbulent boundary layer. Note the slight increase in $u'_c$ on the stagnation line ($z/d = 0$) as the stagnation point is approached. A similar increase in longitudinal turbulence upstream of the cylinder is shown by Britter, Hunt & Mumford (1979) for $0 < L/d < 1.25$ and $4.25 \times 10^3 < Re_d < 2.74 \times 10^4$. However, their measurements were made along the stagnation line instead of the vertical direction and the increase in turbulence was found at an $x$-location ($x/d > -1.5$) closer to the stagnation point than our result. They suggested that the longitudinal turbulence on the stagnation line is amplified by the effect of the flow distortion before the turbulent eddy is blocked by the cylinder surface. Since our lengthscale ratio $L/d$ is 0.8, the results in figure 5 are considered to be explainable by the effect of the flow distortion.

The profiles of the mean velocity defect $U_1 (= U_0 - U)$ in the $(x, z)$-plane in the region $10 \leqslant x/d \leqslant 40$ downstream of the cylinder are shown in figure 6, where the ordinate and abscissa axes are normalized by the maximum velocity defect $U_{1c}$ on the centreline and the half-width $b_u$, respectively. The solid line in figure 6 indicates the self-similar profile of the mean velocity defect in the wake of the cylinder, which is defined by the following Gaussian curve (Schlichting 1979, p. 739):

$$U_1/U_{1c} = \exp\{-(\ln 2)(z/b_u)^2\}. \tag{4}$$

It can be seen from figure 6 that the profiles in this experimental region are not self-similar, but tend to approach gradually the Gaussian curve in the downstream direction. The drag coefficient $C_D$, which is determined by the numerical integration of $U_1$, was nearly constant at each measured $x$-location, averaging about 1.27.

Figure 7 shows the $z$-direction profiles of the r.m.s. longitudinal velocity fluctuation $u'$ measured at the same locations as figure 6. The solid and broken lines in this figure indicate similar profiles of $u'$ for negligible free-stream turbulence from Townsend (1976, p. 188) and Yamada *et al.* (1980). To compare free-stream turbulence with this experiment, the results for $u'$ measured at $x/d = 40$ by Komoda (1957) are indicated by the chain line, in which the free-stream turbulence intensity $u'_0/U_0$ was about 0.021 at the cylinder location. Figure 7 shows that the present experimental data have the same tendency as the chain line, that is, the profile decreases monotonically from the centre to the outer edge, without the distinct double-peaks of the solid and broken lines, and then approaches to the level of free-stream turbulence. Therefore, it is suggested that this more homogeneous turbulence distribution may be caused by

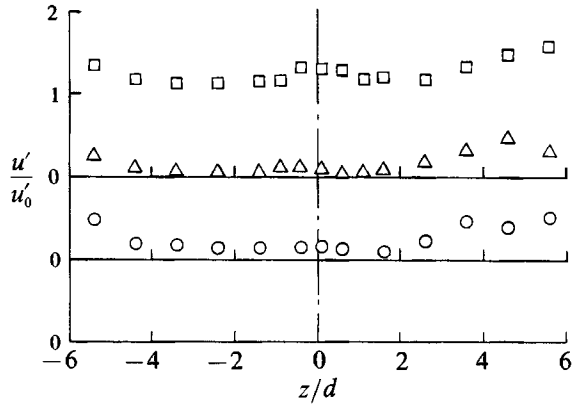


FIGURE 5. Vertical profiles of the r.m.s. longitudinal velocity fluctuation values upstream of the cylinder: ○, $x/d = -5.0$; △, $-3.0$; □, $-1.6$.

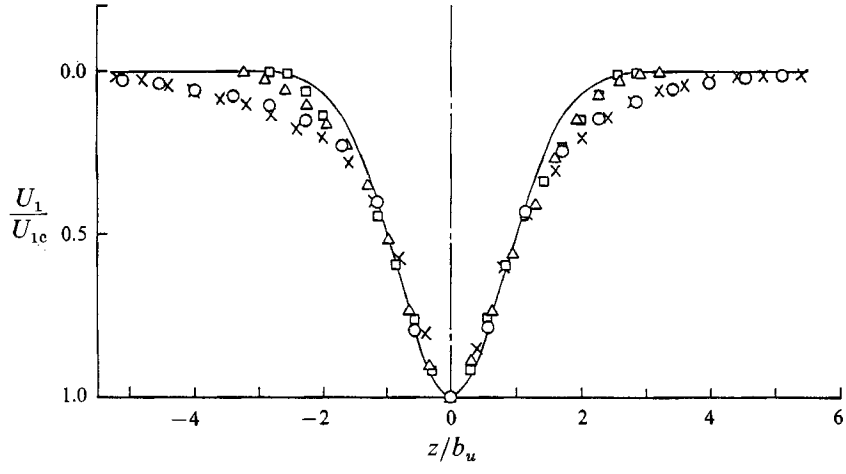


FIGURE 6. Vertical profiles of the mean velocity defect downstream of the cylinder: ○, $x/d = 10$; ×, 20; △, 30; □, 40; —, Gaussian curve.

the change in internal transport processes caused by the free-stream turbulence rather than by the transport process by large eddies. However, its physical interpretation remains unclear, because a simple gradient transport model probably could not be assumed here and the other turbulence components, $v'$ and $w'$, could not be measured in this experiment.

The downstream variations of $U_{1c}$ and $u'_c$ on the centreline of the wake are shown in figure 8. The solid line is an approximate distribution of $U_{1c}$ for negligible free-stream turbulence defined by (Schlichting 1979)

$$\frac{U_{1c}}{U_0} = \frac{C_D}{4\pi^{\frac{1}{2}}}\left(\frac{U_0 d}{\epsilon_0}\right)^{\frac{1}{2}}\left(\frac{x}{d}\right)^{-\frac{1}{2}}, \tag{5}$$

where we assumed $C_D = 1.2$ and $\epsilon_0$, the eddy viscosity, was approximated by the following empirical relation proposed by Schlichting (1979):

$$\epsilon_0 = 0.0222 U_0 C_D d. \tag{6}$$

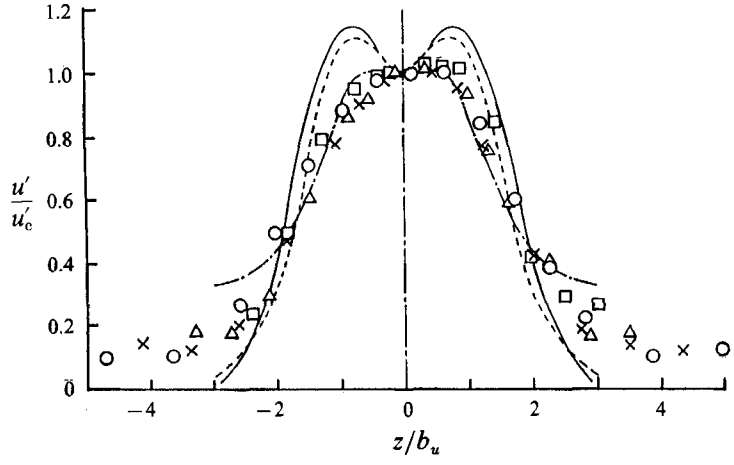


FIGURE 7. Vertical profiles of the r.m.s. longitudinal velocity fluctuation value downstream of the cylinder. Symbols as figure 6; —, Townsend (1976); ----, Yamada *et al.* (1980); –·–·, Komoda (1957).

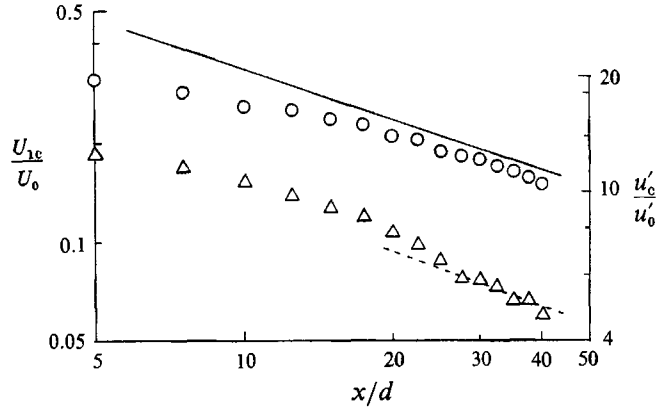


FIGURE 8. Downstream variations of the mean velocity defect (○) and the r.m.s. velocity fluctuation values (△) on the centreline of the wake.

It is found that the experimental values for $U_{1c}$ decrease in parallel with the solid line in the downstream region $20 < x/d$. Furthermore, the comparison with the broken line, which shows the $x^{-\frac{1}{2}}$ power decay law, shows that $u'_c$ tends to decay in proportion to $x^{-\frac{1}{2}}$ in $30 < x/d$.

### 4.2. *Concentration fields*

#### 4.2.1. *Characteristics upstream of and around the cylinder*

Figure 9 shows the decay of the mean concentration $\Gamma_c$ and the r.m.s. concentration fluctuation value $\gamma'_c$ on the centreline of the plume (i.e. the stagnation line) in the region upstream of the cylinder. In this figure, $\Gamma_c$ and $\gamma'_c$ are respectively normalized by $\Gamma_0$ and $\gamma'_0$ (the values at the cylinder location ($x = 0$) in the absence of the cylinder) and both sets of data are plotted on log–log scales. The lower abscissa axis is $(x+x_r)/d$; the distance from the grid. It is often more useful to use dimensionless time $T^*(x) = T(x)\,U_0/a$ (where $a$ is the cylinder radius), and so the upper abscissa axis

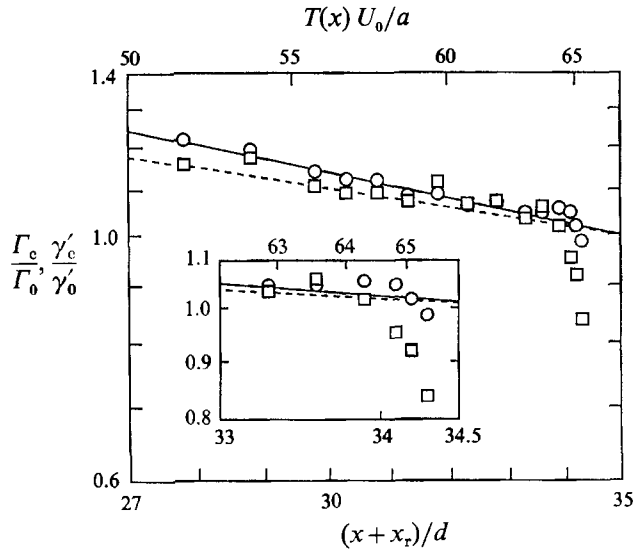


FIGURE 9. Downstream variations of the mean concentration (○) and the r.m.s. concentration fluctuation values (□) on the stagnation streamline. (Inset shows the detail near the stagnation point.)

is $T^*(x)$ for reference. Assuming Taylor's frozen flow hypothesis and the potential velocity along the stagnation line $U^*(x^*) = U(x^*)/U_0 = 1-(1/x^*)^2$ (where $x^* = x/a$), $T^*$ is calculated by the following equation:

$$T^*(x^*) = \int_{-x'^*}^{x^*} \frac{\mathrm{d}x^*}{U^*(x^*)} = x'^* + x^* + \tfrac{1}{2}\ln\left\{\frac{(x^*-1)\,(x'^*+1)}{(x^*+1)\,(x'^*-1)}\right\}, \tag{7}$$

where $x'^* = (x_r - x_n)/a = 66$ is the $x^*$-location of the source exit. Note that $T^*$ differs from the diffusion time for a marked particle which is defined from a Lagrangian point of view. NSM found from the similarity solutions of the $\Gamma$- and $\gamma'$-equations that $\Gamma_c$ and $\gamma'_c$ of a plume from a point source in grid-turbulence decay hyperbolically. The solid and broken lines in this figure approximate each set of data according to a hyperbolic decay law in the region where the effect of the cylinder is negligible and are given by the following equations:

$$\left.\begin{aligned} \Gamma_c/\Gamma_0 &= 40.76\,((x+x_r)/d+5.76)^{-1} \quad \text{(solid line)},\\ \gamma'_c/\gamma'_0 &= 53.30\,((x+x_r)/d+18.3)^{-1} \quad \text{(broken line)}. \end{aligned}\right\} \tag{8}$$

Although it cannot be distinctly seen from the figure, the mean concentration decays in a way roughly similarly to the solid line as the stagnation point is approached. On the other hand, the r.m.s. concentration fluctuation value decays more rapidly in comparison with the broken line in the region $-1.5 < x/d < -0.5$ ($T^* > 64$) near the stagnation point.

The governing equation of the concentration fluctuation variance on the plume centreline is as follows:

$$\frac{\partial\overline{\gamma^2}}{\partial T} = -2\overline{u_i\gamma}\frac{\partial\Gamma}{\partial x_i} - \frac{\partial\overline{u_i\gamma^2}}{\partial x_i} - \epsilon_\gamma, \tag{9}$$

where the left-hand side is expressed in terms of $T' = T^*a/U_0$ defined by (7), the

molecular diffusion term is neglected and $\epsilon_\gamma = 2D_m\overline{(\partial\gamma/\partial x_i)^2}$ is the molecular dissipation of $\overline{\gamma^2}$. By invoking local isotropy and Taylor's frozen flow hypothesis, the dissipation is assumed to be

$$e_\gamma \approx 12D_m\,\overline{\gamma^2}/\lambda_\gamma^2 \approx 6D_m(1/U^2)\,\overline{(\partial\gamma/\partial t)^2}, \tag{10}$$

where $\lambda_\gamma$ is the dissipation scale for the $\gamma$-field (Tennekes & Lumley 1972). The mean and fluctuating concentration fields on the stagnation line of the cylinder are expected to be controlled by the following three mechanisms (Hunt 1990):

($a$) straining of mean flow and increased time of travel;

($b$) change in small-scale turbulence upstream of the cylinder;

($c$) plume flapping caused by large eddies.

Although these mechanisms depend on each other, we consider here their separate effects on the scalar field.

We first consider ($c$). The plume upstream of the cylinder may flap due to large eddies shed from the cylinder (Hunt, Puttock & Snyder 1979), which makes the scalar field more intermittent and thus would cause a decrease in the mean concentration and an increase in the concentration fluctuation. However, this effect would be important only for a narrow plume. In this experiment, such periodic plume flapping was not observed, which can also be seen from the power spectrum of the concentration fluctuation (figure 11) shown later. Effects ($a$) and ($b$) are due to the distortion of striations or blobs of the diffusing matter by the mean straining motion and the turbulence motion, respectively. Hunt & Mulhearn (1973) suggested that, as the stagnation point is approached, the mean concentration in a narrow plume from a point source placed on the stagnation line decays more rapidly than that in the absence of the cylinder. This is supposed to be because of the spanwise and vertical turbulent dispersion of plume which are enhanced due to effect ($a$), especially because of the successively increased time of travel to the cylinder wall. However, this effect on the mean concentration would be important only if the source is near the cylinder so that $b_\Gamma/d \ll 1$. Since the plume width in this experiment is comparable with the cylinder diameter, it is expected that the direct effect of the mean strain on the mean concentration field will be small or negligible as it can be seen from figure 9.

Next, we consider the effect of the turbulence distortion on the concentration fluctuation field. As mentioned in §4.1, the turbulent velocity upstream of the cylinder undergoes a dramatic change due to flow distortion and blocking by the cylinder surface. Britter *et al.* (1979) found that the spectra of the longitudinal and cylinder-axial turbulence components are amplified in a high-wavenumber region by the vortex stretching, independent of the scale ratio $L/d$. Unfortunately, the turbulence spectrum could not be measured in this experiment, but a similar amplification in the high wavenumber spectrum is expected in our experiment because the Reynolds number is of the same order as for their experiment. Since the Schmidt number of our diffusing matter is of the order of $10^3$, the decrease in turbulence scale is considered to lead directly to the decrease in the scale of the scalar field. This attenuation of the scalar scale would continue until an increase in the volume occupied by the diffusing matter and a smoothing of the concentration field occur as a result of the molecular diffusion, which could be accelerated due to an increased concentration gradient by turbulence and mean straining motions.

It must be noted here that a smallest scale of the measured concentration fluctuation could be also limited by the spatial resolution of the concentration-measuring probe, which has an effect similar to the molecular diffusion. Figure 10

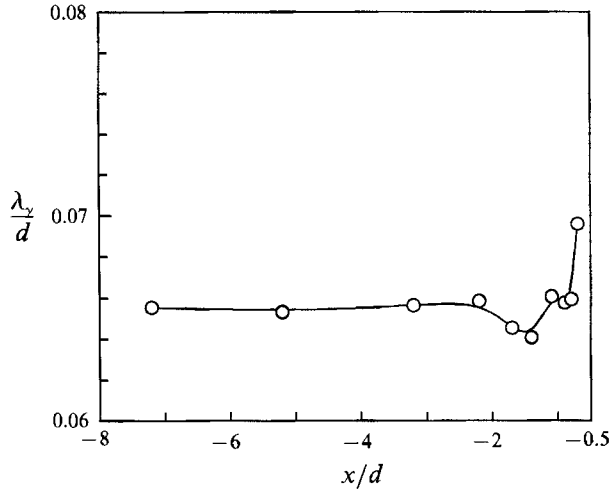


FIGURE 10. Profile of the scalar dissipation scale $\lambda_\gamma$ on the stagnation line.

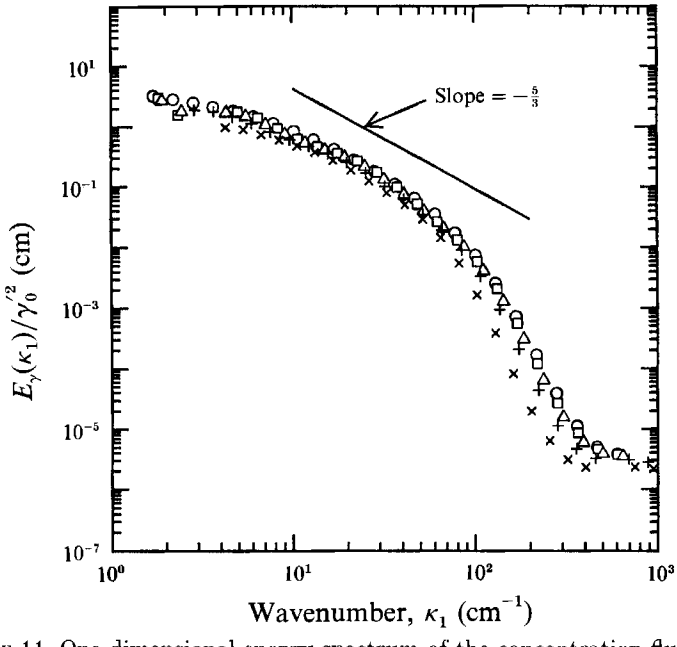


FIGURE 11. One-dimensional energy spectrum of the concentration fluctuation on the stagnation line: ○, $x/d = -3.2$; □, $-1.7$; △, $-1.4$; +, $-0.9$; ×, $-0.7$.

shows the variation of the dissipation scale $\lambda_\gamma$ on the stagnation line, which was estimated by differentiating the time signal of the concentration fluctuation. It can be seen from this figure that before $\lambda_\gamma$ increases near the stagnation point, it decreases in a region $x/d \approx -1.5$ where the incident turbulence begins to be affected by the flow distortion and $\gamma_c'$ begins to decay rapidly. This decrease in $\lambda_\gamma$ is considered to be related to the above-mentioned turbulence change and the mean straining motion upstream of the cylinder, and the subsequent increase in $\lambda_\gamma$ is due to the molecular smearing of the volume occupied by the matter and probably the spatial resolution of the probe. Judging from this behaviour of $\lambda_\gamma$ and (9) and (10), it is suggested that the beginning of the rapid decay of $\gamma_c'$ may be induced by an increase

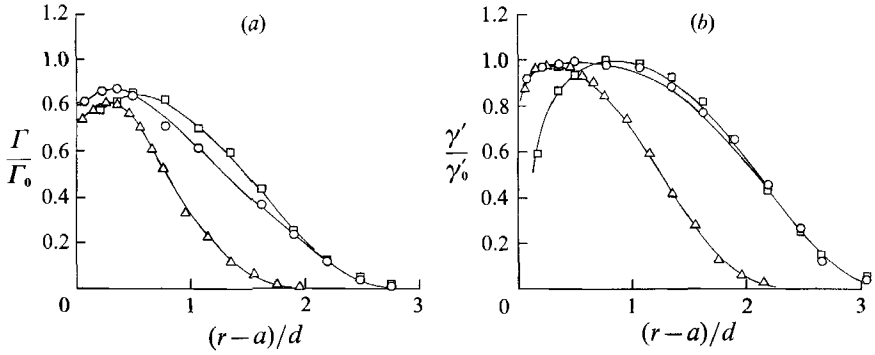


FIGURE 12. Radial profiles of (*a*) the mean concentration and (*b*) the r.m.s. concentration fluctuation values around the cylinder: ○, $\theta = 45°$; △, 90°; □, 135°.

in the molecular dissipation (which includes an effect similar to the probe resolution) through the decrease in $\lambda_\gamma$. Although the dissipation starts to decrease after that, as implied by the increase in $\lambda_\gamma$, the decay of $\gamma'_c$ would be maintained due to the increased time of travel of the diffusing particle which allows more turbulent and molecular diffusion to take place. It should be noted here that Warhaft (1980) found acceleration of the thermal fluctuation decay from a different kind of straining, i.e. by the contraction of the grid-generated turbulence.

Figure 11 shows the variation of the one-dimensional energy spectrum $E_\gamma(\kappa_1)$, normalized by $\gamma'^2_0$, of the concentration fluctuation near the stagnation point. They were estimated from the time series of concentration fluctuation using Taylor's frozen flow hypothesis. In the figure, a line of slope $-\frac{5}{3}$ is also shown for reference. It must be noted that the spectra are accurate up to $\kappa_1 \approx 125$ cm$^{-1}$ beyond which the probe resolution starts to affect their accuracy. Although no appreciable differences are found for the spectra until $x/d = -1.4$, beyond that they begin to decay in a region of high wavenumber, contrary to the expected amplification in the velocity spectrum as the stagnation point is approached. This decay in $E_\gamma$ is related to the increase in $\lambda_\gamma$ shown in figure 10 and could be explained in the same way as before.

Radial profiles of $\Gamma/\Gamma_0$ on the lines $\theta = 45°$, 90° and 135° around the circular cylinder are shown in figure 12(*a*) as a function of $(r-a)/d$. From $\theta = 45°$ to 90°, the width of the profile has reduced and the mean concentrations have also decreased over the whole profile. It is thought that this is caused mainly by the convergence of the streamlines and the spanwise dispersion of the plume, respectively, as the flow passes over the top of the cylinder (Hunt & Mulhearn 1973). However, it must be noted that in spite of this convergence of the streamlines, the half-width (about $0.95d$) of the mean concentration profile on the line $\theta = 90°$ is still larger than that ($0.75d$) in the absence of the cylinder. The profile on the line $\theta = 135°$ is broader than the profile on the line $\theta = 90°$ because of flow separation.

Similar radial profiles of the r.m.s. concentration fluctuation values $\gamma'$ are shown in figure 12(*b*). The distinct characteristic is the rapid decrease in $\gamma'$ near the wall on the line $\theta = 135°$. This decay is mainly related to the recirculating flow inside the separated shear layer. The location of the separation point is estimated as about $\theta = 80°$ from visual observation. Research on a flame holder has shown that both the temperature and concentration of a combustion gas are nearly homogeneous in the recirculating flow region due to the large eddying motion (Tsuji 1977). Therefore, it is suggested that the decrease of $\gamma'$ in figure 12(*b*) could be caused by the homogeneity of the concentration field in the recirculating region.

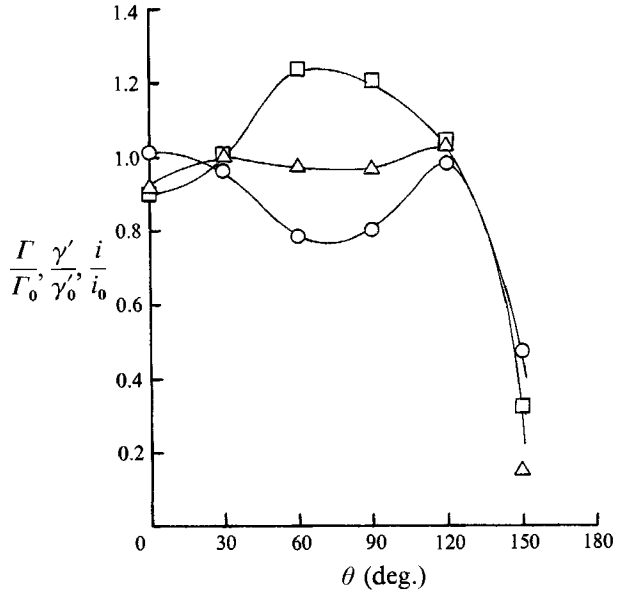


FIGURE 13. Circumferential profiles of the mean concentration (○), the r.m.s. concentration fluctuation values (△) and the relative intensity (□) at $(r-a)/d = 0.3$.

Figure 13 shows circumferential profiles of $\Gamma$, $\gamma'$ and relative intensity $i = \gamma'/\Gamma$ at $(r-a)/d = 0.3$. The mean concentration has a minimum value near the separation point, then increases slightly, and finally decays rapidly for $120° < \theta$. On the other hand, the r.m.s. concentration fluctuation value $\gamma'$ shows no significant change from $\theta = 0°$ to 120°, but in the region $120° < \theta$ it decays steeply. With these circumferential variations of $\Gamma$ and $\gamma'$, the relative intensity $i$ has a maximum value at about $\theta = 80°$.

4.2.2. *Characteristics downstream of the cylinder*

In this section, in view of the intermittency observed in the plume downstream of the cylinder, the characteristics of some conditional statistics will be examined in addition to the conventional mean concentration and r.m.s. fluctuating values.

The conditional mean concentration $\langle\Gamma\rangle$ and the conditional r.m.s. concentration fluctuation value $\langle\gamma'\rangle$ are defined by the following equations using the intermittency function $\tilde{I}(t)$ and the intermittency factor $I_\Gamma$ given in §3:

$$\langle\Gamma\rangle = \overline{\tilde{I}(t)\,\tilde{\Gamma}(t)}/I_\Gamma, \tag{11}$$

$$\langle\gamma'\rangle = [\overline{\tilde{I}(t)\,(\tilde{\Gamma}(t)-\langle\Gamma\rangle)^2}/I_\Gamma]^{\frac{1}{2}}, \tag{12}$$

where overbar denotes the time average. Since $\tilde{\Gamma}(t)$ is zero outside the instantaneous plume, the conventional statistics $\Gamma$, $\gamma'$ and the conditional statistics $\langle\Gamma\rangle$, $\langle\gamma'\rangle$ are related by

$$\Gamma = I_\Gamma\langle\Gamma\rangle \tag{13}$$

and

$$\gamma'^2 = I_\Gamma\langle\gamma'\rangle^2 + I_\Gamma(1-I_\Gamma)\langle\Gamma\rangle^2, \tag{14}$$

respectively (Wilson, Robins & Fackrell 1985). Here $\langle\Gamma\rangle$ and $\langle\gamma'\rangle$ have been determined from (11) and (12) by means of the conditional sampling described in §3.

The mean concentration profiles in the $(x,z)$- and $(x,y)$-planes at various downstream locations behind the cylinder are shown, respectively, in figures 14(*a*)

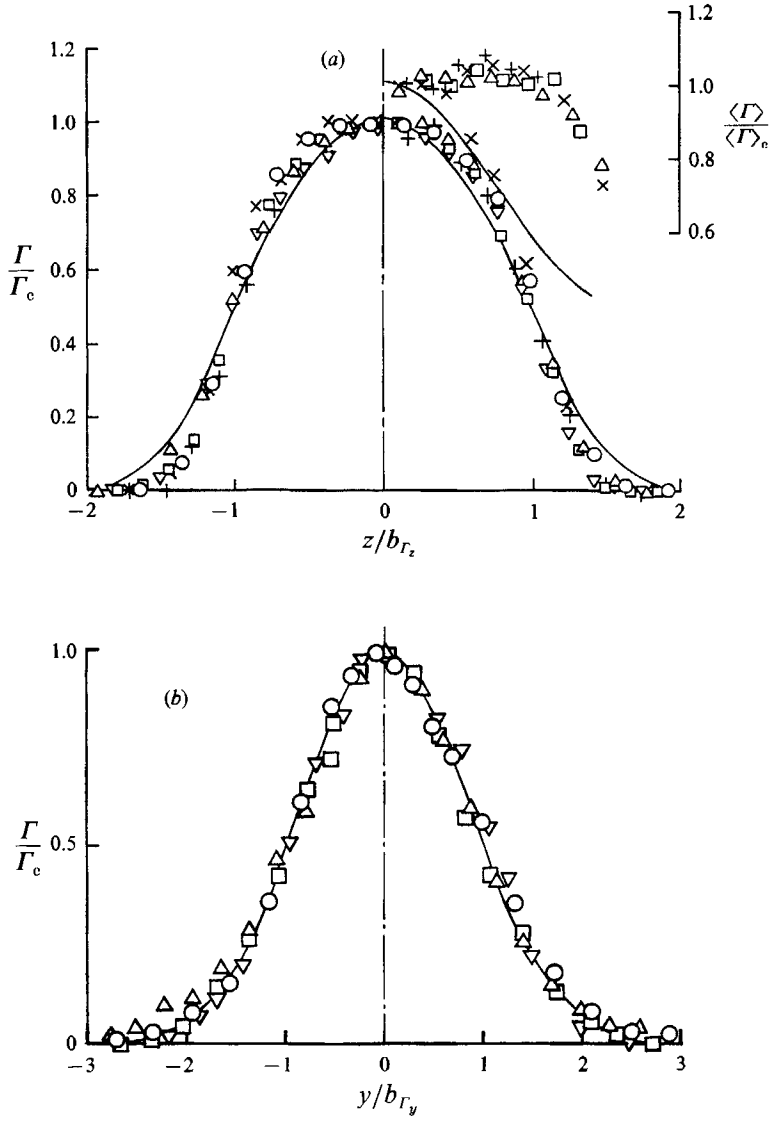


FIGURE 14(*a*) Vertical profiles of the mean concentration downstream of the cylinder: ○, $x/d$ = 5; ×, 10; △, 20; □, 30; ▽, 35; +, 40; —, LaRue & Libby (1974). (*b*) Horizontal profiles of the r.m.s. concentration fluctuation values downstream of the cylinder: ○, $x/d = 20$; △, 30; □, 35; ▽, 40; —, Gaussian curve.

and 14(*b*). In order to clarify the presence of similarity, $\Gamma$ on the ordinate is normalized by $\Gamma_c$ and $z$ and $y$ on the abscissa are normalized by the half-widths $b_{\Gamma_z}$ and $b_{\Gamma_y}$ of the $\Gamma$-profiles in the $(x,z)$- and $(x,y)$-planes, respectively. In figure 14(*a*) the conditional mean concentration profiles in the $(x,z)$-plane are presented only in the region $0 < z$ owing to the symmetry. As shown in the figures, the $\Gamma$-profiles in both $(x,z)$- and $(x,y)$-planes appear to be nearly similar in the region $20 < x/d$. The solid lines in figure 14(*a*) show the self-similar distributions of the conventional mean temperature, and the conditional one measured in the wake of a heated circular cylinder by LaRue & Libby (1974). The present results for $\Gamma$ have a similar tendency to the solid line except for a larger mean concentration gradient at $z/b_{\Gamma_z} = 1.0$, while

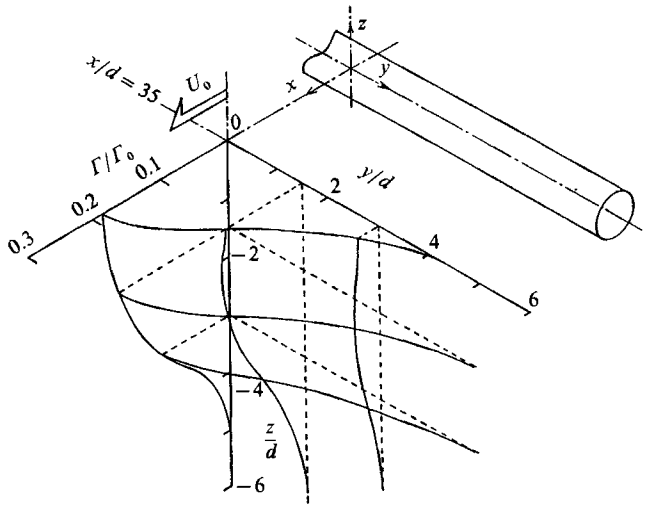


FIGURE 15. Spatial structure of the mean concentration field across the plume at $x/d = 35$.

the results for $\langle \Gamma \rangle$ are completely different from the solid line. This disagreement with regard to $\langle \Gamma \rangle$ may be caused by the fundamental difference of the diffusion process rather than the difference of the Schmidt (or Prandtl) number in the two experiments. In the experiment with the heated cylinder, the diffusing plume develops in the wake with the ambient fluid entrained and its developing region is almost the same as that of the velocity turbulence field if the molecular diffusion is negligible. On the other hand, the present plume, which has developed in grid turbulence, passes around the cylinder and then is entrained into the wake. Thus a more intermittent and meandering plume would be formed in the wake (see figure 2). It should be noted that the uniformity of $\langle \Gamma \rangle$ in the region $0 < z/b_{\Gamma_z} < 1.0$ does not imply homogeneity of the scalar field but is the result of a simple averaging effect due to the large-scale turbulence comparable with the cylinder diameter $d$.

The solid line in figure 14(*b*) shows the Gaussian curve, i.e. the self-similar profile of $\Gamma$ in the absence of the cylinder (NSM), defined by

$$\Gamma/\Gamma_c = \exp\{-(\ln 2)\,(y/b_{\Gamma_y})^2\}. \tag{15}$$

The present similar distribution in the $(x, y)$-plane apparently agrees with the Gaussian curve. This is an interesting result since it will be shown later that the decay rate of $\Gamma_c$ on the centreline and the dispersion rate of the plume in the $(x, y)$-plane are fairly different from those in the absence of the cylinder.

In order to see the spatial structure of the mean concentration field across the plume downstream of the cylinder, the $z$-directional $\Gamma$-profiles on the lines $y/d = 0$, 1.5, 3.0 and the $y$-directional $\Gamma$-profiles on the lines $z/d = 0$, $-1.5$, $-3.0$ at $x/d = 35$, are shown in figure 15. Only the profiles in the regions $z < 0$ and $y > 0$ are exhibited in the figure owing to the symmetry. It is interesting to note that while the $z$-directional profile on $y/d = 0$ has a peak on the centreline, the profiles at $y/d = 1.5$, 3.0 have double-peaks at $z$-locations other than the centreline. This is probably because the $y$-directional $\Gamma$-profile on the line $z/d = -1.5$ is broader than that on the line $z/d = 0$ due to the interference of the upstream plume with the cylinder.

In figures 16(*a*) and 16(*b*), the downstream changes of the $\gamma'$-profiles in the $(x, z)$- and $(x, y)$-planes are presented. As in figure 14(*a*), the profiles of the conditional r.m.s. concentration fluctuation value $\langle \gamma' \rangle$ defined by (12) are given in figure 16(*a*)

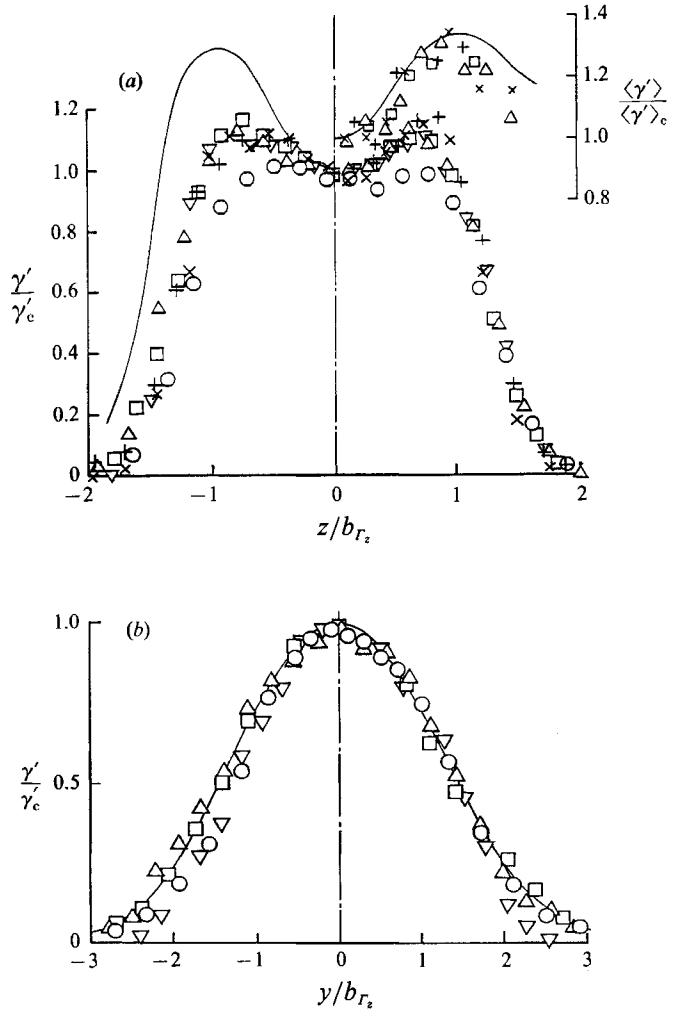


FIGURE 16(*a*) Vertical and (*b*) horizontal profiles of the r.m.s. concentration fluctuation values downstream of the cylinder. Symbols as for figure 14; the solid line in (*b*) is the similarity solution without the cylinder.

only in the region $z > 0$ of the $(x, z)$-plane, and the two solid lines in the region $z < 0$ and $z > 0$ indicate the self-similar distributions of the conventional r.m.s. temperature fluctuation value and the conditional one by LaRue & Libby (1974), respectively. It is found from figure 16 that the $\gamma'$ profiles in both the $(x, z)$- and the $(x, y)$-planes tend to become self-similar in the region $10 < x/d < 40$. Another interesting characteristic in figure 16(*a*) is the double-peaks of the $\gamma'$-profiles in the $(x, z)$-plane. The value and the $z$-location of the double-peaks in the similarity region of $\gamma'$, which are considerably different from those in the solid line, are about 1.13 times $\gamma'_c$ and $z/b_{\Gamma_z} = \pm 0.7$, respectively. In figure 16(*b*), the solid line shows the similarity profile of the concentration fluctuation intensity of a plume in homogeneous isotropic turbulence (NSM). It can be seen that the $y$-directional distribution in the similarity region behind the cylinder agrees with the solid line. But it must be noted that $\gamma'_c$ on the centreline and the $y$-directional half-width $b_{\Gamma_y}$ are considerably different from those without the cylinder (see figures 18 and 20).

Although the physical cause of the double-peaks in this experiment has not been

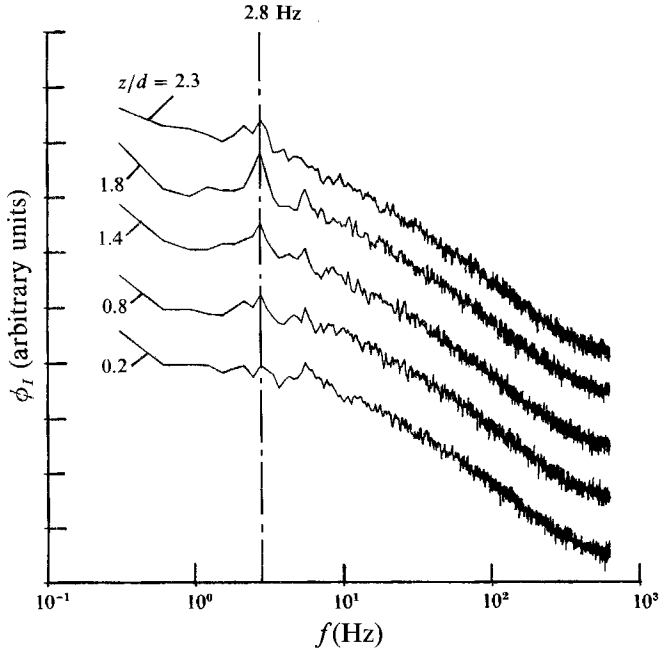


FIGURE 17. One-dimensional power spectrum of the intermittency function of the plume downstream of the cylinder.

clarified, the following two factors are suggested. First, the entrainment of the upstream plume into Kármán vortices may cause large-scale turbulent mixing between the fluid lumps with high- and low-level concentrations, so that the concentration fluctuation in a plume close to the vortex cores is expected to be larger than that on the plume centreline. In fact, the profiles of $\langle\gamma'\rangle$ in figure 16(*a*) have more distinct double-peaks than the profiles of $\gamma'$. Second, a certain meandering (Hanna 1984) of the downstream plume may have resulted due to Kármán vortices formed alternately above and below the centreline in the wake. The meandering of the plume must cause the intermittency of the concentration field. Now, we assume that the effect of the turbulent mixing and the intermittency on the profiles of $\gamma'$ is expressed by the first and second terms of (14), respectively (Wilson *et al.* 1985). In this experiment, the ratio $\alpha$ = (first term)/(second term) = $(\langle\gamma'\rangle/\langle\Gamma\rangle)^2/(1-I_\Gamma)$ of both terms was $\alpha \gg 1$ within the region from $z/b_{\Gamma z} = 0$ to 1.0. Therefore, the effect of the turbulent mixing is considered to be relatively more important than that of the intermittency.

As mentioned above, the meandering of the plume affects the intermittency of the diffusion field, as well as the fluctuating concentration field, greatly (Hanna 1984). In this sense, the present study may be one of the few to investigate the effect of meandering. Since the intermittency function $\tilde{I}(t)$ does not provide information on the amplitude of the concentration fluctuation but only on the detection of concentration, characteristics such as the periodicity of concentration detection due to meandering will appear more clearly in the intermittency function than in the concentration signal itself. Thus, in order to verify the meandering of plume downstream of the cylinder, the distributions of the auto-power spectrum $\Phi_I$ of the intermittency function are shown in figure 17, in which the distributions of $\Phi_I$ at only one $x$-location, $x/d = 10$, are presented. It can be easily seen that the distributions

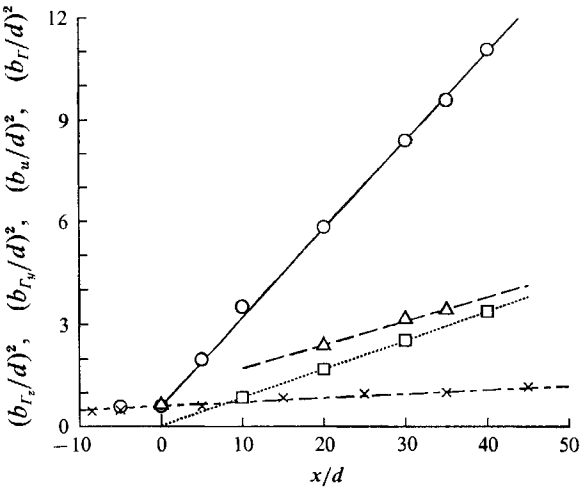


FIGURE 18. Streamwise development of the various half-widths. —, (16) with $A = 0.26$, $x_0 = 2.31$; ---, (16) with $A = 0.069$, $x_0 = 15.0$; ...., (16) with $A = 0.084$, $x_0 = 0.281$; –·–, (16) with $A = 0.012$, $x_0 = 50.4$. ×, $b_\Gamma$ (without cylinder); ○, $b_{\Gamma z}$ (with cylinder); △, $b_{\Gamma y}$ (with cylinder); □, $b_u$ (with cylinder).

of $\Phi_I$ have a peak, which is more distinct in the region $0.8 < z/d < 2.3$. The peak frequency is about 2.8 Hz and this corresponds to the formation frequency $St\,U_0/d = 2.8$ of Kármán vortices obtained from the Strouhal number $St = 0.2$ ($St = 0.2$ is estimated from the Reynolds number $Re_d = 1064$ in this experiment.) Therefore, it can be concluded from figure 17 that the large-eddy structure of Kármán vortices causes the meandering of the plume.

### 4.2.3. *Characteristics on the plume centreline*

In this subsection, the streamwise characteristics of the diffusion field upstream and downstream of the cylinder will be examined.

Figure 18 shows the streamwise development of the squared half-widths $b_{\Gamma z}$ and $b_{\Gamma y}$ of the $\Gamma$-profiles in the $(x,z)$- and $(x,y)$-planes. For comparison, the half-width $b_\Gamma$ of the radial $\Gamma$-profile in the absence of the cylinder (NSM) and the half-width $b_u$ of the $U_1$ profile in the $(x,z)$-plane are also presented. From the approximate self-similarity observed for the $y$- and $z$-directional $\Gamma$-profiles and the $U_1$-profile downstream of the cylinder, the development of each half-width is expected to be described in terms of the following half-power law:

$$(b/d)^2 = A(x/d + x_0), \tag{16}$$

where $b$ represents each half-width, and $A$ and $x_0$ are constants for each half-width. The values of $A$ and $x_0$ corresponding to each half-width, which were determined from the least-squares method, are shown in the caption of the figure and the four lines from these coefficients are shown in the figure. The half-width $b_{\Gamma z}$ downstream of the cylinder spreads much faster than $b_\Gamma$ for the non-disturbed plume. This indicates the significant disturbance effect of the cylinder. The half-width $b_{\Gamma z}$ at the top, $x = 0$, of the cylinder is smaller than that in the absence of the cylinder but this is because the half-width here is defined by the distance from the maximum position of $\Gamma$ instead of the distance from the cylinder surface (see figure 12(*a*)). In the region $20 < x/d$, it can be found from figure 18 that the square of $b_{\Gamma z}$ increases as a nearly

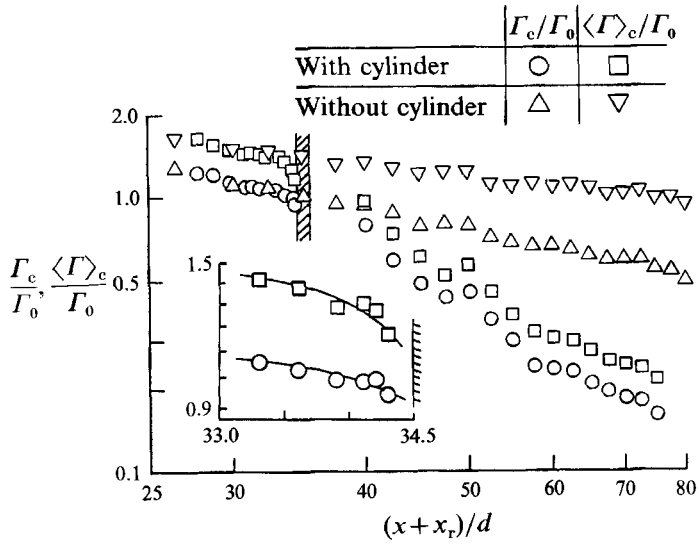


FIGURE 19. Streamwise variations of the conventional and conditional mean concentration. (The insert shows the detail near the stagnation point.)

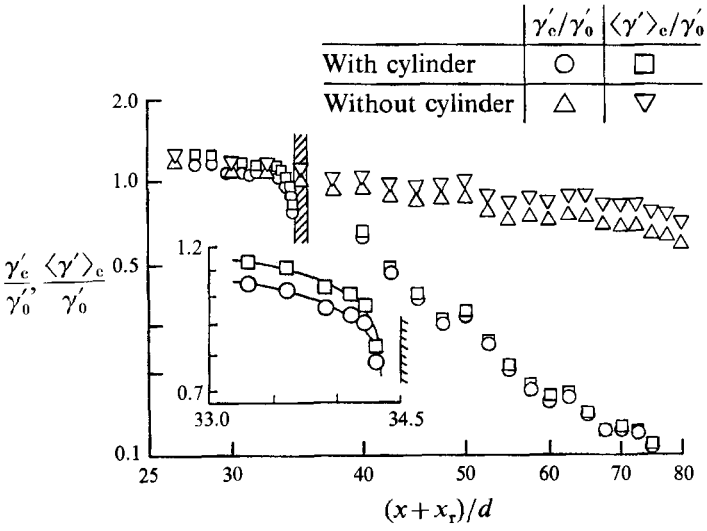


FIGURE 20. Streamwise variations of the conventional and conditional r.m.s. concentration fluctuation values. (The insert shows the detail near the stagnation point.)

1-power law in the downstream direction. On the other hand, the disturbance effect of the cylinder also appears in the $y$-direction as well as the $z$-direction, although $b_{\Gamma y}$ grows more slowly than $b_{\Gamma z}$.

The streamwise variations in the conventional statistics $\Gamma_c$, $\gamma'_c$ and $i_c$ and the conditional statistics $\langle\Gamma\rangle_c$, $\langle\gamma'\rangle_c$ and $\langle i\rangle_c = \langle\gamma'\rangle_c/\langle\Gamma\rangle_c$ on the plume centreline from upstream to downstream of the cylinder are shown, respectively, in figures 19, 20 and 21 with the data for the non-disturbed plume. The area with oblique lines in each figure indicates the space occupied by the cylinder. Here, we focus on the characteristics downstream of the cylinder. (For upstream of the cylinder, see §4.2.1.) From figures 19 and 20, it can be easily seen that $\Gamma_c$ and $\gamma'_c$ in the region

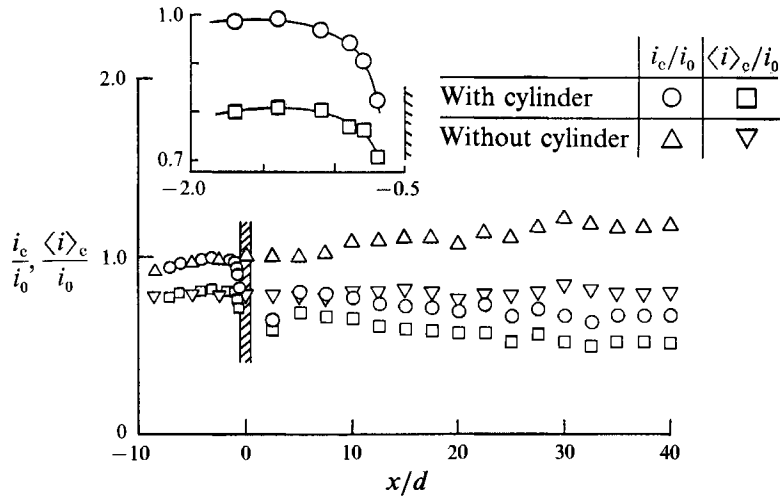


FIGURE 21. Streamwise variations of the conventional and conditional relative intensity. (The insert shows the detail near the stagnation point.)

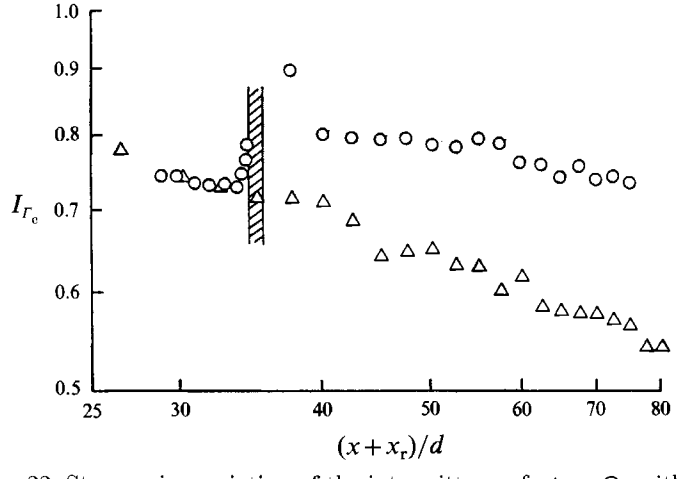


FIGURE 22. Streamwise variation of the intermittency factor: ○, with the cylinder; △, without the cylinder.

downstream of the cylinder decay fairly rapidly in comparison with those of the non-disturbed plume as a result of the spatial expansion of the plume and the mixing encouraged by the disturbance effect of the cylinder. Similar tendencies also appear in the conditional statistics $\langle \Gamma \rangle_c$ and $\langle \gamma' \rangle_c$.

Figure 21 shows that the downstream variation of the relative intensity $i_c$ varies with the presence of the cylinder. The relative intensity in the non-disturbed plume increases in the downstream direction, whereas it decreases in the case of the disturbed plume. It is known that the relative intensity is one of parameters which express the progress of microscopic mixing in the plume, and the progress of mixing is more significant as this value decreases (Georgopoulos & Seinfeld 1986). Therefore, the result of figure 21 indicates that the presence of the cylinder significantly promotes mixing of the matter. Now, in order to consider the difference in the

variation process of the relative intensity between the two cases, we rewrite the relative intensity as follows, using (13) and (14):

$$i = [(\langle i \rangle + 1)^2 / I_\Gamma - 1]^{\frac{1}{2}}. \tag{17}$$

This equation indicates that the mixing of plume has gone through two processes: an increase of $I_\Gamma$ and a decrease of $\langle i \rangle$. From figure 21, $\langle i \rangle_c$ in the disturbed plume decreases in the downstream direction in the region $40 > x/d$, whereas that in the non-disturbed plume is nearly constant. On the other hand, from the streamwise variations of $I_{\Gamma c}$ shown in figure 22, $I_{\Gamma c}$ in the former case is nearly constant, whereas that in the latter case decreases monotonically. Therefore, it can be concluded from (17) that the relative intensity downstream of the cylinder decreases mainly through the decrease of the conditional relative intensity; conversely, in the absence of the cylinder, it increases mainly through the decrease of the intermittency factor.

## 5. Conclusions

The diffusion field of matter, where the plume from a point source in grid-generated turbulence interferes with a circular cylinder of a comparable diameter with the width of the plume, has been examined experimentally including the mean, fluctuating and conditional concentration field. Upstream of the cylinder, it is shown that the disturbance effect of the cylinder appears in the region $-1.5 < x/d < -0.5$. There, the increased travel time as the stagnation point is approached, and the molecular dissipation, which is enhanced by the locally high concentration gradient produced by the mean straining and turbulence motions, cause the rapid decay of $\gamma'$. From $\theta = 45°$ to 90° around the cylinder, the width of the radial $\Gamma$-profiles is reduced and the mean concentration values decrease over all the profiles, mainly by the convergence of streamlines and the spanwise dispersion of the plume. Also, it is found that the effect of the recirculating flow results in a rapid decay of $\gamma'$ near the cylinder wall in the radial profiles. On the other hand, it can be seen that the $\langle \Gamma \rangle$-profiles in the $(x, z)$-plane downstream of the cylinder are nearly constant in the neighbourhood of the plume axis, where the $\Gamma$-profiles in the same plane show flatter shapes than those in the absence of the cylinder and the $\gamma'$-profiles have double-peaks, as do the $\langle \gamma' \rangle$-profiles. Furthermore, a kind of meandering in the downstream plume has been demonstrated from the investigation of the power spectrum of $\tilde{I}(t)$. They are noticeable characteristics caused by the mixing and large-eddy effect of Kármán vortices downstream of the cylinder. The difference in the mixing process of matter on the plume axis with and without the cylinder can be well described by comparing the streamwise variations of $I_{\Gamma c}$ and $\langle i \rangle_c$ in the disturbed plume with those in the non-disturbed plume.

The first author would like to express his special thanks to Professor S. B. Pope in the Department of Mechanical and Aerospace Engineering, Cornell University for reading the manuscript and making a number of helpful comments. The authors are grateful to Professor J. C. R. Hunt in the Department of Applied Mathematics and Theoretical Physics, University of Cambridge for his useful suggestions and to Mr Takehiro Kushida in the Department of Mechanical Engineering, Nagoya University for his technical assistance. The authors also gratefully acknowledge the constructive criticisms of the referees.

## REFERENCES


BILGER, R. W., ANTONIA, R. A. & SREENIVASAN, K. A. 1976 Determination of intermittency from the probability density function of a passive scalar. *Phys. Fluids* **19**, 1471–1474.

BRITTER, R. E., HUNT, J. C. R. & MUMFORD, J. C. 1979 The distortion of turbulence by a circular cylinder. *J. Fluid Mech.* **92**, 269–301.

CHATWIN, P. C. & SULLIVAN, P. J. 1987 Perceived statistical properties of scalars in turbulent shear flows. In *Proc. 6th Symp. Turbulent Shear Flows, Toulouse*, pp. 922–926.

FABRIS, G. 1979 Turbulent temperature and thermal flux characteristics in the wake of a cylinder. *Turbulent Shear Flows 1*, pp. 55–70. Springer.

GEORGOPOULOS, P. G. & SEINFELD, J. H. 1986 Instantaneous concentration fluctuation in point-source plumes. *AIChE J.* **32**, 1642–1654.

HANNA, S. R. 1984 Concentration fluctuations in a smoke plume. *Atmos. Environ.* **18**, 1091–1106.

HUNT, J. C. R. 1985 Turbulent diffusion from sources in complex flows. *Ann. Rev. Fluid Mech.* **17**, 447–485.

HUNT, J. C. R., BRITTER, R. E. & PUTTOCK, J. S. 1979 Mathematical models of dispersion of air pollution around buildings and hills. *Proc. IMA Symp. Math. Modelling Turbulent Diffusion Environment*, pp. 145–200. Academic.

HUNT, J. C. R. & MULHEARN, P. J. 1973 Turbulent dispersion from sources near two-dimensional obstacles. *J. Fluid Mech.* **61**, 245–274.

HUNT, J. C. R., PUTTOCK, J. S. & SNYDER, W. H. 1979 Turbulent diffusion from a point source in stratified and neutral flows around a three-dimensional hill – Part I. Diffusion equation analysis. *Atmos Environ.* **13**, 1227–1239.

KEFFER, J. F., KAWALL, J. G., HUNT, J. C. R. & MAXEY, M. R. 1978 The uniform distortion of thermal and velocity mixing layers. *J. Fluid Mech.* **86**, 465–490.

KIYA, M., SUZUKI, Y., ARIE, M. & HAGINO, M. 1982 A contribution to the free-stream turbulence effect on the flow past a circular cylinder. *J. Fluid Mech.* **115**, 151–164.

KOMODA, H. 1957 On the effect of free-stream turbulence on the structure of turbulent wake. *J. Japan Soc. Aeronautl Engng* **5**, 274–279.

LARUE, J. C. 1974 Detection of the turbulent-nonturbulent interface in slightly heated turbulent shear flows. *Phys. Fluids* **17**, 1513–1517.

LARUE, J. C. & LIBBY, P. A. 1974 Temperature fluctuations in the plane turbulent wake. *Phys. Fluids* **17**, 1956–1967.

NAKAMURA, I., MIYATA, M. & SAKAI, Y. 1983 On a method of the concentration measurement by use of light absorption law. *Bull. JSME* **26**, 1357–1365.

NAKAMURA, I., SAKAI, Y. & MIYATA, M. 1987 Diffusion of matter by a non-buoyant plume in grid-generated turbulence. *J. Fluid Mech.* **178**, 379–403 (referred to herein as NSM).

NAKAMURA, I., SAKAI, Y. & TSUNODA, H. 1989 On conditional statistics of the diffusion field of matter by a point source plume in uniform mean shear flow. *JSME Intl J.* **32**, 180–188.

O'BRIEN, E. E. 1978 Stochastic properties of scalar quantities advected by a non-buoyant plume. *J. Fluid Mech.* **89**, 209–222.

OGAWA, Y. & OIKAWA, S. 1982 A field investigation of the flow and diffusion around a model cube. *Atmos. Environ.* **16**, 207–222.

OGAWA, Y., OIKAWA, S. & UEHARA, K. 1983 Field and wind tunnel study of the flow and diffusion around a model cube – Part II. Nearfield and cube surface flow and concentration patterns. *Atmos. Environ.* **17**, 1161–1171.

PUTTOCK, J. S. 1979 Turbulent diffusion from sources near obstacles with separated wakes – Part II. Concentration measurements near a circular cylinder in uniform flow. *Atmos. Environ.* **13**, 15–22.

PUTTOCK, J. S. & HUNT, J. C. R. 1979 Turbulent diffusion from sources near obstacles with separated wakes – Part I. An eddy diffusivity model. *Atmos. Environ.* **13**, 1–13.

ROBINS, A. G. & CASTRO, I. P. 1977 A wind tunnel investigation of plume dispersion in the vicinity of a surface mounted cube – Part II. The concentration field. *Atmos. Environ.* **11**, 299–311.

SCHLICHTING, H. 1979 *Boundary Layer theory*. McGraw-Hill.

TENNEKES, H. & LUMLEY, J. L. 1972 *A First Course in Turbulence.* MIT Press.

TOWNSEND, A. A. 1976 *The Structure of Turbulent Shear Flow.* Cambridge University Press.

TSUJI, H. 1977 The theory of the combustion phenomenon (16), section 8.2: flame stabilization in high speed air flow. *Sci. of Machine* **29**, 1123–1128 (in Japanese).

WARHAFT, Z. 1980 An experimental study of the effect of uniform strain on thermal fluctuations in grid-generated turbulence. *J. Fluid Mech.* **99**, 545–573.

WILSON, D. J., ROBINS, A. G. & FACKRELL, J. E. 1985 Intermittency and conditionally-averaged concentration fluctuation statistics in plumes. *Atmos. Environ.* **19**, 1053–1064.

YAMADA, H., KUWATA, Y., OSAKA, H. & KAGEYAMA, Y. 1980 Turbulence measurements in a two-dimensional turbulent wake. *Tech. Rep. Yamaguchi Univ.* **2**, 329–339.